

## Revisiting the Global Energy Budget Dynamics with a Multivariate Earth Energy Balance Model to Account for the Warming Pattern Effect

BENOIT MEYSSIGNAC<sup>a</sup>, ROBIN GUILLAUME-CASTEL,<sup>a</sup> AND RÉMY ROCA<sup>a</sup>

<sup>a</sup> LEGOS, Université de Toulouse, CNES, CNRS, IRD, UPS, Toulouse, France

(Manuscript received 6 October 2022, in final form 22 August 2023, accepted 28 August 2023)

**ABSTRACT:** Climate feedbacks are sensitive to the geographical distribution of sea surface temperature (SST). This sensitivity, called the pattern effect, affects the amplitude of the Earth radiative response to anomalies in global mean surface temperature (GMST) and thus is essential in shaping the global energy budget dynamics. Zero-dimensional energy balance models (EBMs) are the simplest representation of the global energy budget dynamics. Many only depend on GMST anomalies and cannot account for the pattern effect explicitly. In EBMs, the pattern effect leads to apparent variations of the global climate feedback parameter  $\lambda$ . Assuming a variable  $\lambda$  in EBMs enables them to more accurately reproduce AOGCM simulations of the GMST anomalies but it leads to variations in  $\lambda$  of  $+>15\%$ . These large variations mean  $\lambda$  is not a constant and the Taylor expansion underpinning EBMs' formulation does not hold, casting doubts on the physical grounding of such EBMs. Here we propose a new EBM based on a multivariate linear Earth radiative response, which depends on both the GMST and the surface warming pattern. The resulting multilinear EBM accurately reproduces AOGCM simulations of anomalies in Earth radiative response and GMST under abrupt  $4\times\text{CO}_2$  forcing. When interpreted in terms of variable  $\lambda$ , the multivariate EBM leads to small variations in  $\lambda$  that are physically consistent with the underpinning Taylor expansion. We analyze with the multivariate framework the variations of the planetary heat uptake  $N$  as a function of the GMST and the pattern of warming through a 3D generalization of the Gregory plot. We show that the apparent nonlinear behavior of the radiative response of the Earth against GMST seen in classical monovariate EBMs (and in classical Gregory plots) can actually be explained by a bilinear dependence of the radiative response of the Earth on the GMST and the pattern of warming. The multivariate EBM further provides an explicit dependence of the global energy budget on the pattern of warming and on the climate state. It has important consequences on the expression of the climate sensitivity.

**KEYWORDS:** Dynamics; Feedback; Stability; Budgets; Climate change; Climate sensitivity

### 1. Introduction

Climate is dynamic and its dynamics are complex to represent because climate is an open system (i.e., continuously exchanging energy with the exterior) with subtle interplay of a large number of feedbacks and forcings. Some feedbacks may only become relevant in the future, or may no longer be relevant, and some changes may be nonlinear, abrupt, or irreversible, which further complicates the representation of the climate system's dynamics. The simplest representation of the climate system's dynamics is the zero-dimensional energy balance model, which builds on the first law of thermodynamics to derive a representation of the dynamics of the global energy budget. Budyko (1969) and Sellers (1969) introduced a linear approximation of the zero-dimensional energy balance model (EBM) to represent, at first order, the time changes in the global mean surface temperature driven by changes in the solar forcing. Today, these EBMs

are still essential tools used either in hierarchies of models to interpret more complex models such as comprehensive atmosphere–ocean general circulation models (AOGCMs, e.g., Armour et al. 2013; Geoffroy et al. 2013a,b; Held et al. 2010) or to interpret observations and deduce fundamental characteristics of the current climate system such as the global climate feedback parameter  $\lambda$ , the transient climate response (e.g., Gregory and Forster 2008), or the equilibrium climate sensitivity (ECS; e.g., Chenal et al. 2022; Lewis and Curry 2018; Sherwood et al. 2020).

EBMs assume to the first order that the radiative response of the Earth to an anomalous radiative forcing is linear with the change in global mean surface temperature (the linear coefficient being  $\lambda$ , the global feedback parameter). Under such an assumption, the radiative response of Earth depends only on the globally averaged surface temperature anomalies. However, recent advances in theory (e.g., Winton et al. 2010; Armour et al. 2013; Geoffroy et al. 2013b,a; Bloch-Johnson et al. 2020), climate model simulations (Murphy 1995; Murphy and Mitchell 1995; Senior and Mitchell 2000; Gregory and Andrews 2016; Andrews et al. 2018; Andrews and Webb 2018; Dong et al. 2019; Marvel et al. 2018; Paynter and Frölicher 2015; Zhou et al. 2017), and observations (Loeb et al. 2018; Fueglistaler 2019; Meyssignac et al. 2023) show that Earth's radiative response is sensitive to the geographical pattern in surface temperature and that this pattern effect is large and plays a role in the global energy budget. Because EBMs depend only on global mean surface temperature, EBMs cannot account explicitly for the pattern effect in the

 Denotes content that is immediately available upon publication as open access.

 Supplemental information related to this paper is available at the Journals Online website: <https://doi.org/10.1175/JCLI-D-22-0765.s1>.

*Corresponding author:* Benoit Meyssignac, benoit.meyssignac@legos.obs-mip.fr

Earth radiative response. Instead, the pattern effects show up in EBMs through an apparent time dependence of  $\lambda$ . The time dependence of  $\lambda$  means that the intensity of the various climate feedbacks vary over time in response to changes in the geographical distribution of the sea surface temperature.

Allowing  $\lambda$  to be variable with time increases significantly an EBM's capacity to interpret the global energy budget dynamics either observed or simulated by AOGCMs. For example, it enables EBMs to better represent the global mean surface temperature evolution simulated by AOGCMs. It also enables one to explain why  $\lambda$  is different in AOGCM simulations of the historical period or in historical observations compared to  $\lambda$  at equilibrium in AOGCM simulations of an abrupt doubling of atmospheric CO<sub>2</sub> concentration (e.g., [Armour 2017](#)). But, at the same time, allowing  $\lambda$  to be variable leads to physical inconsistencies in the EBMs' formulation. Indeed, EBMs with a variable global feedback parameter show large variations of  $>+15\%$  in  $\lambda$  (sometimes up to  $+1.0 \text{ W m}^{-2} \text{ K}^{-1}$ ) [see [section 2](#); see also [Andrews et al. \(2018\)](#) their Fig. 2f for examples]. Sometimes, it also leads to extreme nonphysical estimates of  $\lambda$  (see [section 2](#)). These large variations and extreme values in  $\lambda$  are inconsistent with the linear approximation which leads to the EBM formulation in the first place. It casts doubts on the physical grounding of EBMs with a variable  $\lambda$  (see [section 2](#)).

In this study we revisit the development of EBMs and propose a new approach to account for the pattern effect in EBMs. Our approach consists in developing a multivariate EBM to account for the dependence of the radiative response of Earth on both the global mean surface temperature and the geographical distribution of the surface temperature (see [section 3](#)). In [section 4](#) we numerically verify that the linear assumptions that are underpinning the multivariate EBM are satisfied. We show with a numerical integration that under abrupt quadrupling of atmospheric CO<sub>2</sub> concentration the climate system remains in a multilinear regime and that the multivariate EBM is sufficient to accurately reproduce the global mean surface temperature evolution. In [section 5](#) we use the multivariate EBM to explain the apparent variations in the global climate feedback parameter  $\lambda$ . We show that the multivariate EBM leads to a new expression of  $\lambda$ . This new expression of  $\lambda$  shows small departures around a mean value which are consistent with the linear approximation that leads to the multivariate EBM formulation in the first place. We also show that the apparent variations of  $\lambda$  actually correspond to a linear dependence of  $\lambda$  on the warming pattern through a 3D version of the Gregory plot. In [section 6](#) we discuss the differences between the classical version of the EBM with a varying  $\lambda$  and the new multivariate EBM. In particular, we discuss their different expression of  $\lambda$ . In [section 7](#) we discuss how the multivariate EBM compares with a number of bivariate EBMs that have been proposed recently to account for the pattern effect.

## 2. Classical global energy budget with a monovariate radiative response of Earth

Let  $N$  be the radiation imbalance at the top of the atmosphere (TOA) between the net longwave radiation flux  $I$  and the net shortwave radiation flux  $S$ :  $N = S + I$  (we adopt the

convention that net incoming radiation is positive and thus  $N$  is positive for a net energy gain of the climate system). Both the net shortwave and the net longwave radiation fluxes can be partitioned into a forced part (coming from the solar and the aerosol forcing for example in the case of the shortwave flux, and coming from the CO<sub>2</sub> radiative forcing for example for the longwave flux) and a response part such that  $N$  now reads

$$N = S + I = F + R, \quad (1)$$

where  $F$  is the sum of all the forcing ( $F$  typically amounts to several hundreds of watts per square meter) and  $R$  is the radiative response of Earth to this forcing (by definition  $R = N - F$  and  $R$  amounts to several hundreds of watts per square meter as well, in general).

We assume that the climate system is not perturbed for a time long enough that it reaches a steady state (subscript "ss"). In this steady state,

$$N_{\text{ss}} = S_{\text{ss}} + I_{\text{ss}} = F_{\text{ss}} + R_{\text{ss}} = 0. \quad (2)$$

Let  $T_{\text{ss}}$  be the global mean surface temperature and  $R_{\text{ss}}$  be the radiative response of the Earth that characterize this steady state. Note that, at steady state,  $R_{\text{ss}} = -F_{\text{ss}}$ .

Now let  $\tilde{F}$  be a forcing perturbation (i.e., a sustained perturbation) to this energy balance (hereafter, in all notations, the tilde indicates anomalies with respect to the steady state ss). The term  $\tilde{F}$  is an unspecified source of radiative forcing with units of watts per square meter. It could be caused by a change in greenhouse gases concentrations, a change in the solar forcing, a volcanic eruption, or other causes. In response to the applied forcing perturbation  $\tilde{F}$ , the Earth radiation balance will adjust and the surface temperature will change. The changes in surface temperature are determined by the dynamics of the energy budget of the atmosphere and the ocean mixed layer (on interannual and longer time scales the ocean mixed layer is in equilibrium with the atmosphere so we consider they form the same subsystem whose temperature is characterized by the global mean surface temperature). If the system consisting of the atmosphere and the ocean mixed layer is assumed to have some thermal inertia  $C$ , the equation that describes the time-dependent evolution of the global annual-mean surface temperature  $T$  is

$$C \frac{dT}{dt} + H = N = S + I = R + F_{\text{ss}} + \tilde{F}, \quad (3)$$

where  $H$  represents the heat exchange with the ocean layers that are below the mixed layer, and  $R$  is the radiative response of Earth: it corresponds to the steady-state radiative response plus the changes at TOA in both  $I$  and  $S$  that are caused by the radiative anomaly  $\tilde{F}$ . Note that  $R$  includes the Planck response of the climate system as well as the climate feedbacks (mainly the water vapor feedback, the lapse rate feedback, the surface albedo feedback, and the cloud feedback). For small departures in  $T$ ,  $R$  is assumed to be monovariate and to only depend on the global mean surface temperature  $T$  (e.g., [Budyko 1969](#); [Sellers 1969](#); [Gregory et al. 2004](#); [Roe 2009](#)).

Let  $\tilde{F}$  be sufficiently small that it causes changes in  $T$  that are small compared to  $T_{ss}$ , that is,  $T = T_{ss} + \tilde{T}$  with  $\tilde{T} = o(T_{ss})$ . The radiative response of Earth  $R$  can then be linearized around the steady-state temperature  $T_{ss}$  with the following equation:

$$R(T_{ss} + \tilde{T}) = R(T_{ss}) + \tilde{R} = R_{ss} + \tilde{R}, \quad (4)$$

where  $\tilde{R}$  is the anomaly in Earth radiative response. Note that  $\tilde{R}$  is small compared to  $R_{ss}$  as Eq. (4) is a Taylor expansion. The term  $\tilde{R}$  follows:

$$\tilde{R} = R - R_{ss} = \frac{dR}{dT} \Big|_{T=T_{ss}} \tilde{T} + o\left(\frac{\tilde{T}}{T_{ss}}\right) \simeq \lambda \tilde{T}. \quad (5)$$

Equation (5) is the equation of the linear tangent Earth radiative response at the point  $T_{ss}$ . The term  $\lambda = dR/dT|_{T=T_{ss}}$  is a negative constant called the global climate feedback parameter [see also Gregory et al. (2004) for a simple method to evaluate the relationship between  $\tilde{R}$  and  $\tilde{T}$  and to derive an estimate of  $\lambda$ ].

Now, we introduce the linear tangent Earth radiative response around the steady state  $T_{ss}$  [i.e., Eqs. (4) and (5)] into the Earth energy budget [Eq. (3)] to derive the linear tangent Earth energy budget under the radiative anomaly  $\tilde{F}$ :

$$C \frac{d\tilde{T}}{dt} - \lambda \tilde{T} = \tilde{F} - \tilde{H}. \quad (6)$$

Equation (6) is the linear approximation of the dynamics of the global Earth energy budget around the point  $T_{ss}$  [see also Roe (2009) for another method based on the feedback analysis to derive Eq. (6)]. It is referred to, in the literature, as the 0D energy balance model (e.g., North and Kim 2017).<sup>1</sup>

Recent research showed that climate feedbacks' intensity is sensitive not only to the global mean surface temperature anomaly but also to the geographical pattern of the surface temperature and so is the Earth radiative response anomaly  $\tilde{R}$  (e.g., Winton et al. 2010; Armour et al. 2013; Senior and Mitchell 2000; Gregory and Andrews 2016; Andrews et al. 2018; Loeb et al. 2018, and many others). However, in Eq. (5),  $\tilde{R}$  only depends on the global mean surface temperature anomaly. As a consequence, the pattern effect leads to apparent variations in  $\lambda$  in the energy budget represented by Eq. (6) [see also, e.g., Gregory and Andrews (2016) and Andrews et al. (2018)].

To account for the pattern effect, authors (e.g., Murphy 1995; Murphy and Mitchell 1995; Senior and Mitchell 2000;

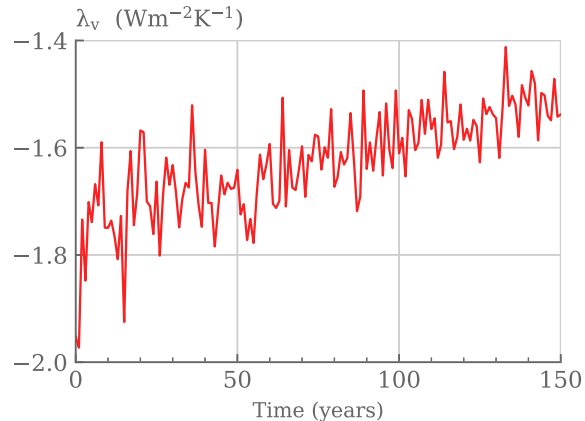


FIG. 1. Variations of  $\lambda_v$  across time computed from the classical monovariate global energy budget (i.e.,  $\lambda_v = \tilde{R}/\tilde{T}$ ) in CCSM4.0 simulation under an abrupt 4xCO<sub>2</sub> concentration.

Armour et al. 2013, and many others) have directly added a variable  $\lambda$  in the expression of the Earth radiative response anomaly [Eq. (5)] leading to the following equation:

$$\tilde{R} \simeq \lambda_v \tilde{T}, \quad (7)$$

where the index  $v$  has been added to  $\lambda$  to showcase that  $\lambda$  is now considered as a variable.

This new expression of the Earth radiative response anomaly leads to a monovariate energy balance model with a variable  $\lambda_v$ :

$$C \frac{d\tilde{T}}{dt} - \lambda_v \tilde{T} = \tilde{F} - \tilde{H}. \quad (8)$$

Equations (7) and (8) are the general representation of the classical energy balance model with a variable  $\lambda_v$  (see, e.g., Armour et al. 2013; Rohrschneider et al. 2019; Dong et al. 2019). This representation reproduces the variations of the Earth radiative response anomaly under a changing global surface temperature along with a changing pattern in surface temperature (because it is built to do so). However, it leads to large variations in  $\lambda_v$  of  $>+15\%$  (see Fig. 1). For other models than CCSM4.0 it leads to even larger variations in  $\lambda_v$  of  $>+30\%$  [see Fig. 2f in Andrews et al. (2018)]. These large variations in  $\lambda_v$  mean the system gets out of the region of validity of the Taylor expansion made in Eq. (5). As a consequence the linearized expression of the radiative response of the Earth in Eq. (7) is no more valid along with the EBM represented by Eq. (8).

This issue becomes critical when  $\tilde{T} \sim 0$  while  $\tilde{R}$  remains sizeable because then  $\lambda_v$  [which is defined as  $\lambda_v = \tilde{R}/\tilde{T}$  by Eq. (7)] get to extreme values. This is well illustrated by atmospheric general circulation model (AGCM) simulations developed to estimate the Green's functions that relate the global Earth radiative response anomaly to local anomalies in surface temperature (Zhou et al. 2017; Dong et al. 2019). These simulations provide an estimate of the Earth radiative response anomaly to localized patch of sea surface temperature (SST) of a few

<sup>1</sup> Note that Budyko (1969) and Sellers (1969) derived a similar equation to Eq. (6) but they used a slightly different approach. They derived Eq. (6) under the hypothesis that  $R$  is, to the first order, linear with surface temperature; i.e.  $R = \text{cste} + \lambda T$ . This hypothesis is not mentioned in our development from Eqs. (2) to (5) and seems at first sight useless to get to Eq. (6). But Budyko and Sellers' hypothesis is actually implicit in the linearization of the radiative response around  $T_{ss}$ , in Eq. (5). Indeed, by integrating Eq. (5) with respect to  $T$  we find that  $R = \text{cste} + \lambda T$  that precisely corresponds to Budyko and Sellers' hypothesis.

kelvins applied on a  $40^\circ$  longitude  $\times 15^\circ$  to  $25^\circ$  latitude zone. In these simulations the global mean temperature change is close to zero ( $<0.0005$  K, because the anomaly of temperature that is imposed is small and very localized; see Fig. 2a) but the global Earth radiative response anomaly in response to some of the localized patch in SST is significant (because of the pattern effect; see Fig. 2b), leading to extremely high (or low when negative) values of  $\lambda_v$  (see Fig. 2c). For example, AGCM simulations with a patch of SST of 1.5 K localized in the western tropical Pacific lead to an estimate of  $\lambda_v$  of  $-15$  to  $-20$   $\text{W m}^{-2} \text{K}^{-1}$ . The same AGCM, forced with a patch of SST of 1.5 K localized in the eastern tropical Pacific, leads to an estimate of  $\lambda_v$  of  $+10$  to  $+15$   $\text{W m}^{-2} \text{K}^{-1}$ . These extremes values of  $\lambda_v$  are one order of magnitude out of the region of validity of the Taylor expansion made in Eq. (5). It illustrates the physical inconsistency of Eq. (7).

### 3. Revisiting the global energy budget with a multivariate radiative response of the Earth

Here, we develop a multivariate version of the equations of the 0D energy balance model to properly account for the dependence of the Earth radiative response anomaly  $\tilde{R}$  on the pattern effect. We assume that the radiative response of the Earth  $R$  depends on both the global surface temperature  $T$  and the geographical pattern of surface temperature  $\mathbf{p}$  (where the vector  $\mathbf{p}$  is a multivariate metric for the geographical pattern in surface temperature, which is independent from the global mean temperature  $T$ ). So,  $R$  is a multivariate function that depends on  $T$  and on  $\mathbf{p}$ . Let  $\tilde{F}$  be sufficiently small that it causes a small anomaly in  $T$  (i.e.,  $T = T_{ss} + \tilde{T}$ ) and a small anomaly in  $\mathbf{p}$  (i.e.,  $\mathbf{p} = \mathbf{p}_{ss} + \tilde{\mathbf{p}}$ ). The radiative response of the Earth  $R$  can then be linearized around the steady state ( $T_{ss}$ ,  $\mathbf{p}_{ss}$ ) with the following equation:

$$\begin{aligned} \tilde{R} &= R(T_{ss} + \tilde{T}, \mathbf{p}_{ss} + \tilde{\mathbf{p}}) - R(T_{ss}, \mathbf{p}_{ss}) \\ &= \nabla R|_{(T, \mathbf{p})=(T_{ss}, \mathbf{p}_{ss})} \cdot (\tilde{T}, \tilde{\mathbf{p}}) + o(\tilde{T}, \tilde{\mathbf{p}}) \\ &\simeq \partial_T R|_{(T, \mathbf{p})=(T_{ss}, \mathbf{p}_{ss})} \tilde{T} + \nabla_p R|_{(T, \mathbf{p})=(T_{ss}, \mathbf{p}_{ss})} \cdot \tilde{\mathbf{p}} \\ &\simeq \lambda_{ss} \tilde{T} + \nabla_p R|_{(T, \mathbf{p})=(T_{ss}, \mathbf{p}_{ss})} \cdot \tilde{\mathbf{p}} \end{aligned} \quad (9)$$

Equation (9) is the equation of the multivariate linear tangent Earth radiative response around the point ( $T_{ss}$ ,  $\mathbf{p}_{ss}$ ). Equation (9) shows that, in the multivariate approach, the linear tangent Earth radiative response is the sum of two terms: 1) the change in the radiative response of the climate system under the increase in global mean surface temperature (represented by the term  $\lambda_{ss} \tilde{T}$ ) and 2) the change in the radiative response of the climate system under a changing pattern of surface temperature while keeping the global mean surface temperature constant (represented by the term  $\nabla_p R|_{(T, \mathbf{p})=(T_{ss}, \mathbf{p}_{ss})} \cdot \tilde{\mathbf{p}}$ ).

Now, we introduce the linear tangent Earth radiative response around the steady state ( $T_{ss}$ ,  $\mathbf{p}_{ss}$ ) [Eq. (9)] into the Earth energy budget [Eq. (3)] to derive the multivariate linear tangent Earth energy budget under the radiative anomaly  $\tilde{F}$ :

$$C \frac{d\tilde{T}}{dt} - \lambda_{ss} \tilde{T} - \nabla_p R|_{(T, \mathbf{p})=(T_{ss}, \mathbf{p}_{ss})} \cdot \tilde{\mathbf{p}} = \tilde{F} - \tilde{H}. \quad (10)$$

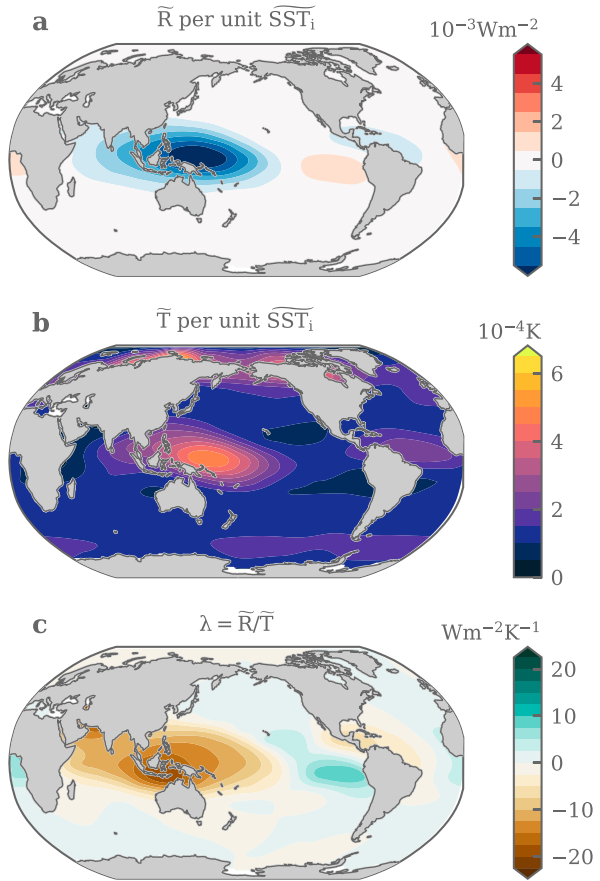


FIG. 2. (a) Global radiative response of Earth, (b) local surface temperature response, and (c) global feedback parameter derived from the classical monovariate global energy budget (i.e.,  $\lambda = \tilde{R}/\tilde{T}$ ) in response to a localized patch of SST of 1.5 K applied on a  $40^\circ$  longitude  $\times 15^\circ$  to  $25^\circ$  latitude zone simulated with the Community Atmosphere Model 4 (CAM4) by Dong et al. (2019). Figure adapted from Dong et al. (2019).

Note that Eq. (10) is derived from the total differential of the radiative response of Earth [Eq. (9)]. To confirm Eq. (10), we tested another approach with the feedback analysis method (see appendix). It leads to the same result and thus gives confidence in Eq. (10) as the equation of the multivariate energy budget.

### 4. Numerical validation of the multivariate global energy budget

#### a. Numerical validation of the multivariate linearization of the Earth radiative response

The main assumption underpinning the formulation of the multivariate energy budget described in Eq. (10) is the linear approximation made in the Taylor expansion of the radiative response of Earth in Eq. (9). In this section we verify numerically that this linear assumption holds in AOGCM simulations of the climate response to a quadrupling of  $\text{CO}_2$  atmospheric concentration.

To do so, we compute the radiative response of the Earth from the mean surface temperature anomaly and the warming pattern of an abrupt 4xCO<sub>2</sub> simulation, using Eq. (9) and we compare it with the radiative response estimated as the difference between the Earth energy imbalance  $N$  and the radiative forcing  $\bar{F}$  of the same abrupt 4xCO<sub>2</sub> simulation.

The radiative forcing  $\bar{F}$  is taken from the sstClim4xCO<sub>2</sub> and sstClim simulations of the Coupled Model Intercomparison Project phase 5 (CMIP5; Taylor et al. 2012). In the sstClim4xCO<sub>2</sub> simulation the atmospheric concentration in CO<sub>2</sub> is abruptly quadrupled and the SST is kept at its monthly-varying preindustrial climatological mean. In this simulation the radiative response anomaly is null because the SST is kept at the level of the preindustrial control simulation so the TOA radiative imbalance anomaly  $\bar{R}$  gives an estimate of the forcing  $\bar{F}$  (which is here the forcing induced by the abrupt quadrupling of atmospheric CO<sub>2</sub> concentrations). We use the TOA radiative imbalance anomaly of the sstClim4xCO<sub>2</sub> simulation as a direct estimate of  $\bar{F}$ , after removing the drift and bias from the sstClim experiment [method from Hansen et al. (2005)]. Note that we do not account for impacts of changes in land temperature, which could slightly change the estimates of the forcing (e.g., Andrews et al. 2021). This impacts only marginally the results shown further. We find  $\bar{F} = 8.84 \text{ W m}^{-2}$ .

We consider as a metric for the warming pattern, any local departure of the SST around the global mean SST. With such a metric,  $\mathbf{p}$  is the vector  $(\overline{\text{SST}}_i)_{i=1,n}$  (where  $\overline{\text{SST}}_i$  indicates the local departure in SST around the global mean at the geographical location  $i$ ) and the pattern effect of Eq. (9) reads as follows:

$$\nabla_p R|_{(T, \mathbf{p})=(T_{ss}, \mathbf{p}_{ss})} \cdot \tilde{\mathbf{p}} = \sum_{i=1}^n \partial_{\overline{\text{SST}}_i} R|_{(T, \mathbf{p})=(T_{ss}, \mathbf{p}_{ss})} \overline{\text{SST}}_i. \quad (11)$$

We can estimate the pattern effect described in Eq. (11) from AOGCM Green's function experiments. Indeed, Green's function experiments provide an estimate of the Earth radiative response anomaly to localized patch of sea surface temperature (i.e.,  $\text{SST}_i$ ) of a few kelvins. However, in Green's function experiments the global mean surface temperature change  $\bar{T}$  is not exactly zero because the small localized patch of SST is not compensated for in the rest of the ocean by a small decrease in SST. It means that the radiative response of Earth in Green's function experiments has a small residual term, which is due to the increase in global mean surface temperature  $\bar{T}$  that has to be corrected for, in order to evaluate the radiative response that is associated with the pattern of warming only. We correct for this effect and evaluate the pattern effect from Green's function experiment in the following way:

$$\begin{aligned} & \nabla_p R|_{(T, \mathbf{p})=(T_{ss}, \mathbf{p}_{ss})} \cdot \tilde{\mathbf{p}} \\ &= \sum_{i=1}^n \partial_{\overline{\text{SST}}_i} (R_{GF_i} - \lambda_{ss} \overline{\text{SST}}_{GF_i})|_{(T, \mathbf{p})=(T_{ss}, \mathbf{p}_{ss})} \overline{\text{SST}}_i, \end{aligned} \quad (12)$$

where GF<sub>i</sub> refers to the Green's function experiment that imposes a patch of SST on the location  $i$  and the overbar indicates the global mean.

To estimate  $\lambda_{ss}$  we need an experiment with the same setup as the preindustrial control run on which we impose a global mean surface warming without any change in the pattern of SST [see the definition of  $\lambda_{ss}$  in Eq. (9)] in order to keep the preindustrial SST pattern unchanged. No additional change in the SST pattern means zero additional changes in the local departures of the SST around the global mean [see Eq. (11)]. This means that the surface warming we impose has to be a uniform warming. There is no such experiment available in the CMIP suite. But we can build one using the piSST and the piSST-p4K AGCM simulations from the pilot experiments (Chadwick et al. 2017) of the Cloud Feedback Model Intercomparison Project phase 3 (CFMIP3; Webb et al. 2017). In the piSST simulation, an AGCM model is forced with the preindustrial atmospheric constituents and, at the surface boundary, the preindustrial monthly-varying SSTs are imposed. The radiative response anomaly in the piSST simulation is therefore the same as the radiative response anomaly in the preindustrial control run. In the piSST-p4K simulation, an AGCM model is forced with the preindustrial atmospheric constituents and, at the surface boundary, the preindustrial monthly-varying SSTs are imposed along with an additional uniform SST increase of +4 K. The difference in the radiative response anomaly between the piSST and the piSST-p4K simulations is the radiative response induced by the uniform increase in SST. Thus, we estimate  $\lambda_{ss}$  as the ratio of the radiative response anomaly difference between the piSST and the piSST-p4K simulations over the equivalent global mean surface temperature difference. We find  $\lambda_{ss} = -2.22 \text{ W m}^{-2} \text{ K}^{-1}$ .

We now use the estimate of  $\lambda_{ss}$  and Eq. (12) to estimate the linearized radiative response of Earth on an abrupt 4xCO<sub>2</sub> simulation and we compare it with the total radiative response of Earth estimated as  $N - \bar{F}$ . Only the CAM4 model (Neale et al. 2010) provides at the same time the outputs of the piSST simulation, the piSST-p4K simulation, and the Green's function experiments. So, the results can only be shown for this model.

Figure 3 shows the comparison between the linearized estimate of the radiative response of the Earth and the total radiative response of the Earth for the CCSM4.0 abrupt 4xCO<sub>2</sub> simulation (the CCSM4.0 abrupt 4xCO<sub>2</sub> simulation is the coupled simulation under abrupt 4xCO<sub>2</sub> concentrations that uses CAM4 as atmospheric model). There is a good agreement in Fig. 3 between both estimates, at all time scales from 0 to 150 years, within the internal variability of the simulated radiative response of Earth. The good agreement suggests that the radiative response of Earth is multilinear over a large range of surface warming of several kelvins and nonlinearities remain small in the Earth radiative response variability, even under 5 K of warming.

Despite the good agreement, there is a small discrepancy between the linearized estimate of the radiative response and the total radiative response of CCSM4.0 which arises on decadal time scales from 130 to 150 years of simulation. This discrepancy is of the order of a few tenths of watts per square meter (see Fig. 3). We suspect three reasons for this discrepancy: 1) the linear assumption of the Green's functions is probably not good enough to capture the exact radiative

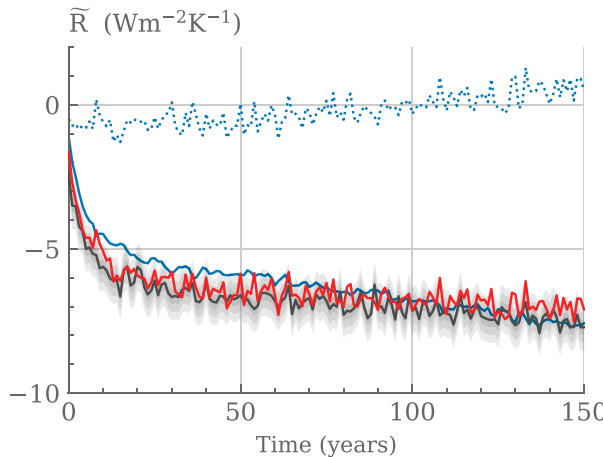


FIG. 3. Linearized global radiative response of Earth (red) from Eq. (9) against total global radiative response (black) estimated as  $N - F$  in CCSM4.0 abrupt 4xCO<sub>2</sub> simulation. The linearized global radiative response of Earth is decomposed into the radiative response to the global mean surface temperature anomaly (plain blue) and the radiative response to the pattern of warming (dashed blue). The shading around the total global radiative response indicates the associated internal variability estimated at 1 $\sigma$ , 2 $\sigma$ , and 3 $\sigma$  from the CCSM4.0 preindustrial control run.

response over land because it assumes the land surface temperature is a response to SST changes only, which is obviously partial; 2) the Green's functions we are using here have fixed sea ice so the impact of sea ice on the radiative response is not addressed in our study; and 3) nonlinearities in the radiative response to global mean surface warming and to pattern changes could also start to arise after a few kelvins of global warming and explain part of the discrepancy.

Note that a previous study based on the classical monovariate energy budget finds a larger discrepancy between the linearized radiative response and the total radiative response (Dong et al. 2019). This is because here we decompose the total SST into a globally uniform warming plus the departures around the uniform warming. We account for the globally uniform warming with a global-mean SST warming experiment (amip-4K) and we account for the departures around the uniform warming with Green's functions. In contrast Dong et al. (2019) accounts for the entire warming with Green's functions only. Zhang et al. (2023) develop a similar approach as we do here, in their Eq. (5) and their Fig. 4. They confirm that accounting separately for the uniform warming with a uniform warming experiment leads to a better fit of the radiative response of Earth. Note also that, although Zhang et al. (2023) develop a similar approach as we do here [in their Eq. (5) and their Fig. 4] the fit between the linearized radiative response and the total radiative response is slightly better in our case. We suspect this is because we use 40-yr-long Green's functions with an amplitude of 1.5–3.5 K rather than 10-yr-long ones with an amplitude of 1.5 K. This difference plays an important role (see Zhang et al. 2023, their Figs. 9a and 12a).

### b. Numerical validation of the multivariate global energy budget

We now numerically validate the multivariate energy budget proposed in Eq. (10). To do so, we integrate the global energy budget represented in Eq. (10) to estimate the global mean surface temperature changes  $\tilde{T}$  under the forcing of an abrupt 4xCO<sub>2</sub> concentration and we compare it with the changes in  $\tilde{T}$  simulated by the CCSM4.0 model under the same forcing.

To derive estimates of  $\tilde{T}$  from Eq. (10), we need to expand the term  $\tilde{H}$ , which represents the heat exchange with ocean deep layers. The term  $\tilde{H}$  can be represented by adding a deep ocean layer (i.e., below the mixed layer).

With a deep ocean layer, Eq. (10) reads:

$$\begin{cases} C \frac{d\tilde{T}}{dt} = \tilde{F} + \lambda_{ss} \tilde{T} + \nabla_p R|_{(T,p)=(T_{ss},p_{ss})} \cdot \tilde{\mathbf{p}} - \gamma_1 (\tilde{T} - \tilde{T}_d) \\ C_d \frac{d\tilde{T}_d}{dt} = \gamma_1 (\tilde{T} - \tilde{T}_d) \end{cases}, \quad (13)$$

where  $C_d$  is the heat capacity of the deep ocean layer and  $\gamma$  is the diffusion coefficient between the surface layer and the deep ocean layer. This model is similar to the one in Geoffroy et al. (2013a,b), but with a different radiative response. To compare this two-layer model with the CCSM4.0 simulation, we evaluate the parameters  $C$ ,  $C_d$ , and  $\gamma$  using a differential evolution optimal algorithm (Storn and Price 1997) that minimizes the distance between the integrated Eq. (10) and the CCSM4.0 output. We find  $C_s = 8.32 \text{ W yr m}^{-2} \text{ K}^{-1}$ ,  $C_d = 107.7 \text{ W yr m}^{-2} \text{ K}^{-1}$ , and  $\gamma = 0.86 \text{ W m}^{-2} \text{ K}^{-1}$  for CCSM4.0. These values are consistent with the assessed ranges of  $C_s$ ,  $C_d$ , and  $\gamma$  in AOGCMs (Geoffroy et al. 2013a,b).

Now that the parameters of the two-layer model are set, we integrate the multivariate global energy budget and assess its capacity to reproduce the global mean surface temperature anomaly of the CCSM4.0 abrupt 4xCO<sub>2</sub> simulation. Figure 4 shows the estimate of  $\tilde{T}(t)$  computed from the two-layer model compared to the  $\tilde{T}(t)$  output of the CCSM4.0 abrupt 4xCO<sub>2</sub> simulation. Figure 4 shows an agreement of both estimates at all time scales between 0 and 150 years, within the internal variability of  $\tilde{T}(t)$  at the 5%–95% confidence level. As for the radiative response of Earth, we find that the multivariate linear global energy budget represented by Eq. (10) is sufficient to reproduce the first 150 years of global mean surface temperature change in response to abrupt 4xCO<sub>2</sub> forcing.

### 5. Explaining the variations in $\lambda$ with the multivariate global energy budget

Here, we consider the radiative response of Earth as a function of the global feedback parameter  $\lambda$  and the global mean surface temperature  $T$ . We assume that the climate feedback parameter  $\lambda$  varies so the radiative response of Earth now reads:

$$R = R(T, \lambda_v). \quad (14)$$

As before, the index  $v$  indicates that  $\lambda$  is a variable. We use Eq. (14) to interpret the multivariate global energy budget in

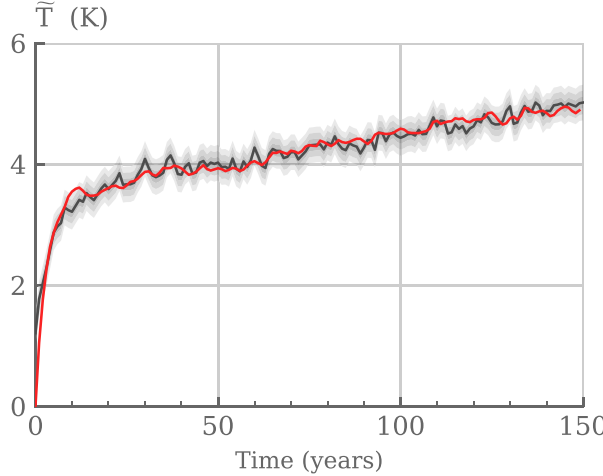


FIG. 4. Abrupt 4xCO<sub>2</sub> global mean surface temperature emulated by the two-layer model [Eq. (13) in red] against the output of CCSM4.0 abrupt 4xCO<sub>2</sub> simulation (black). The gray shaded areas indicate the internal variability of the CCSM4.0 simulation of global mean surface temperature estimated from the CCSM4.0 pi-control simulation. The levels of gray indicate the internal variability at 1 $\sigma$ , 2 $\sigma$ , and 3 $\sigma$ .

terms of variable  $\lambda_v$ . We choose the variable  $\lambda_v$  as a metric  $p$  of the pattern effect and we calculate the linearized radiative response of the Earth by making the multivariate Taylor expansion of the radiative response of the Earth around the point ( $T = T_{ss}$ ,  $\lambda_v = \lambda_{ss}$ ) as follows:

$$\begin{aligned} \tilde{R} &= R(T_{ss} + \tilde{T}, \lambda_{ss} + \tilde{\lambda}_v) - R(T_{ss}, \lambda_{ss}) \\ &\simeq \partial_T R|_{(T, \lambda_v) = (T_{ss}, \lambda_{ss})} \tilde{T} + \partial_{\lambda_v} R|_{(T, \lambda_v) = (T_{ss}, \lambda_{ss})} \tilde{\lambda}_v. \end{aligned} \quad (15)$$

The first term of the right-hand side of Eq. (15) is the radiative response to a uniform warming while the second term is the radiative response to a change of surface temperature pattern without any uniform warming. The term  $\partial_T R|_{(T, \lambda_v) = (T_{ss}, \lambda_{ss})}$  represents the climate feedback parameter of the system at  $(T_{ss}, \lambda_{ss})$  under the condition  $\tilde{\lambda}_v = 0$  (i.e., under the condition of uniform warming). In other words,  $\partial_T R|_{(T, \lambda_v) = (T_{ss}, \lambda_{ss})} = \lambda_{ss}$ . The term  $\partial_{\lambda_v} R|_{(T, \lambda_v) = (T_{ss}, \lambda_{ss})}$  is a constant that is homogeneous at a temperature. By definition, it is the temperature of the system when there is only a pattern effect and there is no uniform warming (i.e., under the condition  $\tilde{T} = 0$ ). In other words,  $\partial_{\lambda_v} R|_{(T, \lambda_v) = (T_{ss}, \lambda_{ss})} = T_{ss}$ .

Substituting this expression in Eq. (15) leads to the following linearized radiative response of Earth:

$$\tilde{R} \simeq \lambda_{ss} \tilde{T} + T_{ss} \tilde{\lambda}_v, \quad (16)$$

where  $T_{ss}$  is the temperature of the reference steady state and  $\tilde{\lambda}_v$  is the anomaly in  $\lambda_v$  with respect to the reference steady state  $\lambda_{ss}$  (i.e.,  $\lambda_v = \lambda_{ss} + \tilde{\lambda}_v$ ). The anomalies in the radiative feedback parameter  $\tilde{\lambda}_v$  are directly related to the pattern effect. Indeed, equalizing the expression of the radiative response in Eq. (16) with the expression of the radiative

response in Eq. (11) shows that the anomalies in the radiative feedback parameter are driven by the anomalies in the local SST in the following way:

$$\tilde{\lambda}_v = \frac{1}{T_{ss}} \sum_{i=1}^n \partial_{\text{SST}_i} R|_{(T, p) = (T_{ss}, p_{ss})} \widetilde{\text{SST}}_i. \quad (17)$$

Note that in Eq. (16) the pattern effect on the radiative response (which is  $T_{ss} \tilde{\lambda}_v$ ) explicitly depends on the temperature of the steady state  $T_{ss}$ , suggesting the pattern effect could be different for different climate states. This dependence should not be interpreted as a physical dependence. It is only a mathematical technicality that comes from the Taylor development of the linear tangent plane around the point  $(\lambda_{ss}, T_{ss})$ . Indeed, if we replace in Eq. (16)  $\tilde{\lambda}_v$  by its definition [which is given by Eq. (17)], then the dependence of the pattern effect on  $T_{ss}$  vanishes and the pattern effect only depends on the local dependence in SST around the global mean, as expected.

The new formulation of the Earth radiative response anomaly in Eq. (16) leads to the following new expression of the dynamics of the global energy budget with a variable  $\lambda_v$ :

$$C \frac{d\tilde{T}}{dt} - \lambda_{ss} \tilde{T} - T_{ss} \tilde{\lambda}_v = \tilde{F} - \tilde{H}. \quad (18)$$

To analyze the dependence of the radiative response anomaly of the Earth  $\tilde{R}$  on  $\tilde{T}$  and  $\tilde{\lambda}_v$  and to test the linear relation proposed in Eq. (16) we plot  $N = \tilde{R} + \tilde{F}$  against  $\tilde{T}$  and  $\tilde{\lambda}_v$  in the CCSM4.0 abrupt 4xCO<sub>2</sub> simulation. Here  $N$  is estimated from the difference between incoming and outgoing radiation at TOA and  $\tilde{\lambda}_v$  is estimated with Eq. (17). Figure 5a shows the 3D plot of  $N$  against  $\tilde{T}$  and  $\tilde{\lambda}_v$ . Figure 5a is a generalized 3D version of the Gregory plot (Gregory et al. 2004). It shows how the anomaly of the radiative response of the Earth  $\tilde{R}$  decreases from  $\tilde{F}$  to 0 with time as a function of  $\tilde{T}$  and  $\tilde{\lambda}_v$ . We added on Fig. 5a the plane defined by Eq. (16) (pink shaded area). This pink plane is the plane of the bilinear tangent radiative response of the Earth at the point  $(T_{ss}, \lambda_{ss})$ . If the points of the CCSM4.0 are along this plane it means that the radiative response of the Earth is bilinear with respect to  $\tilde{T}$  and  $\tilde{\lambda}_v$ . As a matter of fact, the points of the CCSM4.0 are all along the plane even when the surface warming reaches high anomalies such as 5 K (see Fig. 5c, which shows an azimuthal rotation of the 3D plot that enables to view the 3D plot along the linear tangent plane). Figure 5c confirms that the bilinear Eq. (16) is an accurate approximation of the CCSM4.0 even for warming up to 5 K.

Figure 5b shows the projection of the 3D plot onto the plane  $\tilde{\lambda}_v = 0$ . Note the pink shaded area in Fig. 5b. It shows the projection of the linear tangent plane of Eq. (16) onto the plane  $\tilde{\lambda}_v = 0$ . Figure 5b is the classical Gregory plot (Gregory et al. 2004) of the monovariate Earth radiative response. It shows that if  $\tilde{R}$  is considered as a monovariate function of  $\tilde{T}$  then  $\tilde{R}$  is a nonlinear function of  $\tilde{T}$ ; that is, increments in  $\tilde{R}$  tend to be smaller for the same increment in  $\tilde{T}$  when the system gets close to equilibrium (see, e.g., Andrews et al. 2015). However, the 3D plot in Fig. 5a reveals that this apparent nonlinear behavior of the monovariate Earth radiative

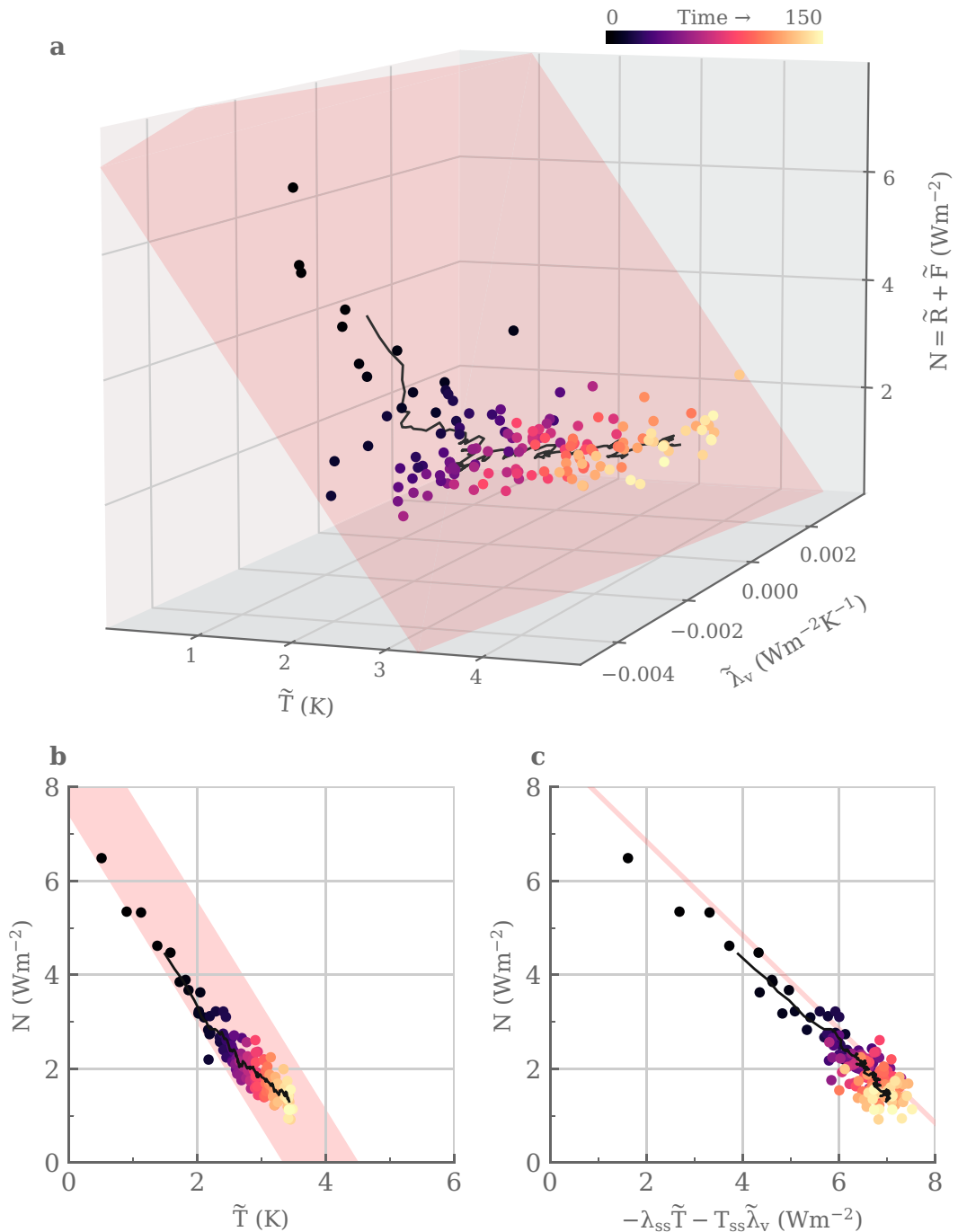


FIG. 5. Earth energy imbalance  $N = \tilde{R} + \tilde{F}$  against  $\tilde{T}$  and  $\tilde{\lambda}_v$  in the CCSM4.0 abrupt 4xCO<sub>2</sub> simulation. (a) 3D plot of  $N$  against  $\tilde{T}$  and  $\tilde{\lambda}_v$ . Each point represents a year in the CCSM4.0 simulation. The black line is a 10-yr running mean. The color indicates the time in the abrupt 4xCO<sub>2</sub> simulation. The pink shaded area indicates the plane of the linear tangent radiative response of Earth at the point  $(T_{ss}, \lambda_{ss})$ . (b) Projection of the 3D plot on the plane  $\tilde{\lambda}_v = 0$ . So (b) shows the classical Gregory plot (Gregory et al. 2004) of CCSM4.0. The pink shaded area shows the projection of the linear tangent plane onto the plane  $\tilde{\lambda}_v = 0$ . (c) Azimuthal rotation of the 3D plot of  $\arctan(\lambda_{ss}/T_{ss})$ , which enables us to view the 3D plot along the edge of the linear tangent plane. The pink line indicates the projection of the linear tangent plane. Note the small bias between the points and the pink line. This bias is due to a small error in the estimate of the radiative forcing anomaly. A video version of the plot is available in the online supplemental material.

response anomaly seen on the Gregory plot of Fig. 5b is explained by the dependence of  $\tilde{R}$  on a second variable, which is the pattern of warming measured here by  $\tilde{\lambda}_v$ . This results shows that the bilinear approximation of Eq. (16) explains the apparent nonlinear behavior observed in the Gregory plot up to 5 K of warming.

## 6. Difference between the multivariate energy budget and the classical energy budget: New estimates of $\lambda_v$ and its variations

The classical monovariate energy budget [Eq. (8)] and the multivariate energy budget [Eq. (18)] accurately reproduce AOGCMs' simulations of the Earth radiative response anomaly and of the global mean surface temperature of the Earth to forcing anomalies. Indeed, if we derive a two-layer model from Eq. (8), as we did with Eq. (13) in the previous section, we will find a fit with the abrupt-4xCO<sub>2</sub> simulations of  $\tilde{T}(t)$  as good as the fit we find in Fig. 4 with Eq. (13). This is expected because both the classical and the multivariate energy budgets are constructed to simulate accurately the Earth radiative response anomaly and the global mean surface temperature.

However, each energy budget shows a different relationship between the changes in the radiative response of Earth and the changes in surface temperature [cf. Eq. (7) to Eq. (16)]. In the multivariate framework, the Earth radiative response anomaly induced by a perturbation can be interpreted as the sum of two terms: 1) the radiative response anomaly induced by a change in global mean surface temperature under the constant climate feedback parameter ( $\lambda_{ss}\tilde{T}$ ) and 2) the radiative response anomaly induced by a change in the global climate feedback under constant global mean surface temperature ( $T_{ss}\tilde{\lambda}_v$ ) [see Eq. (16)]. This expression of  $\tilde{R}$  is very different from the expression of  $\tilde{R}$  in the classical monovariate energy budget [Eq. (7)] where the effects of the global mean surface temperature and the climate feedback parameter on the Earth radiative response anomaly are multiplicative. As a consequence, the multivariate framework yields to a different estimate of the climate feedback parameter  $\lambda_v(t)$ . Indeed, while the classical framework shows variations in  $\lambda_v(t)$  of up +0.3 W m<sup>-2</sup> K<sup>-1</sup> the multivariate framework shows variations in  $\lambda_v(t)$  of only a few 0.001 W m<sup>-2</sup> K<sup>-1</sup> under the same abrupt 4xCO<sub>2</sub> forcing (see Fig. 6).

Note that in the case of the multivariate framework the variations in  $\lambda_v(t)$  are two orders of magnitude smaller than  $\lambda_{ss}$ , confirming the hypothesis that  $\tilde{\lambda}_v$  is small compared to  $\lambda_{ss}$ . In addition, in the multivariate framework  $\lambda_v$  is defined when  $\tilde{T} = 0$ ; in such a case  $\lambda_v(t) = \lambda_{ss}$ , which is indeed the global climate feedback parameter of the piControl simulation. The term  $\lambda_v$  is also well defined when  $T \rightarrow 0$ . Indeed, in the case of Green's functions, for example where  $\tilde{T} \sim 0$ , then  $\lambda \sim \lambda_{ss}$ , which is physically consistent with the linear hypothesis underpinning the multivariate energy budget (see Fig. 7). This physical consistency with the underpinning linear assumption gives confidence in the physical groundings of the multivariate energy budget and in the new estimates of the global climate feedback parameter.

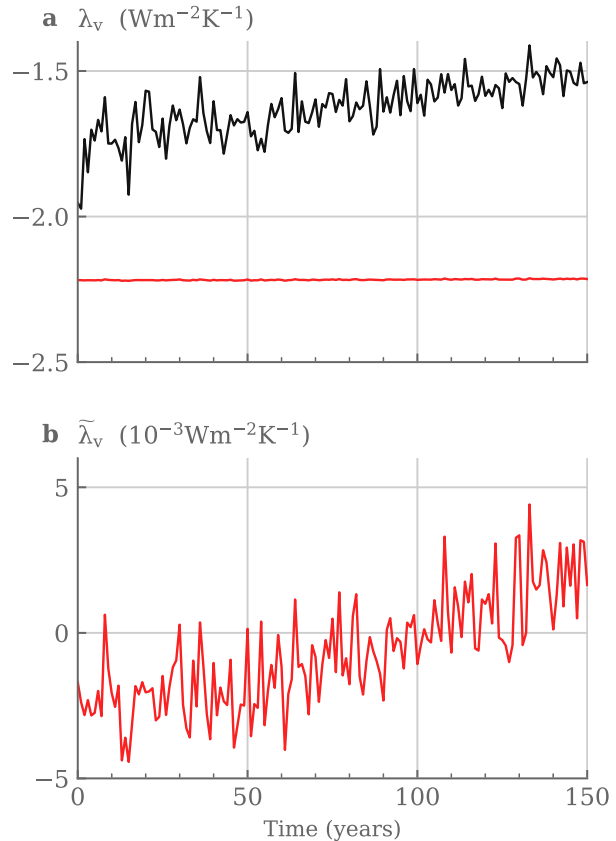


FIG. 6. (a) Global climate feedback parameter estimated from the classical monovariate framework, i.e.,  $\lambda_v(t) = \tilde{R}/\tilde{T}$  (black line) and global climate feedback parameter estimated from the multivariate framework, i.e.,  $\lambda_v(t) = \lambda_{ss} + \tilde{\lambda}_v$  (red line). (b) Zoom on the anomalies in the global climate feedback parameter  $\tilde{\lambda}_v(t)$  estimated with the multivariate framework using Eq. (17). The estimates are derived from the CCSM4.0 abrupt-4xCO<sub>2</sub> simulation.

The new definition of the global climate feedback parameter derived from the multivariate EBM leads to new estimate of the equilibrium climate sensitivity (ECS). Indeed, the ECS derived from the asymptotic solution of the multivariate energy budget reads as follows:

$$ECS = -\frac{\tilde{F}(2xCO_2)}{\lambda_{ss}} - T_{ss} \frac{\tilde{\lambda}_{v\infty}}{\lambda_{ss}}, \quad (19)$$

where  $\tilde{\lambda}_{v\infty}$  is the anomaly in global climate feedback parameter when the climate system has reached a new steady state. Interestingly, the multivariate framework shows that the ECS depends on both the climate state  $\lambda_{ss}$  and the pattern of SST  $\tilde{\lambda}_{v\infty}$ . This opens the possibility to quantitatively evaluate the dependence of the ECS upon both the climate state and the pattern effect at the same time. It is out of the scope of this paper to explore all the consequences of the multivariate energy budget formulation on the estimate of the ECS. This will be done in a further study dedicated to the climate sensitivity.

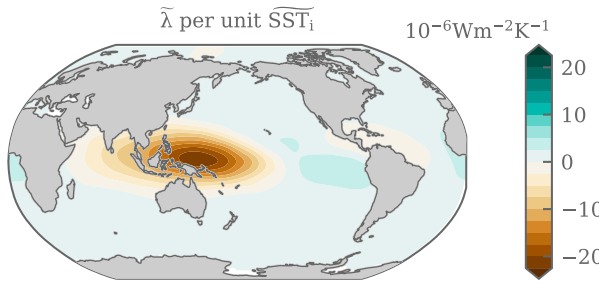


FIG. 7. Global feedback parameter derived from the multivariate energy budget [Eq. (16)] in response to a localized patch of SST of 1.5 K applied on a  $40^\circ$  longitude  $\times$   $15^\circ$  to  $25^\circ$  latitude zone, estimated from the CAM4 Green's function experiment (Dong et al. 2019);  $\lambda_{ss} = -2.22 \text{ W m}^{-2} \text{ K}^{-1}$ ,  $T_{ss} = 291.2 \text{ K}$ .

## 7. Comparison of the multivariate energy budget with previous bivariate frameworks

Several alternative frameworks to the classical monovariate energy budget have been proposed in the literature in order to account for the effect of the SST pattern on the Earth radiative response anomaly. We count three major alternative frameworks, namely the heat uptake efficacy framework (Winton et al. 2010; Held et al. 2010; Geoffroy et al. 2013b,a; Jimenez de la Cuesta 2023), the warm pool temperature framework (Fueglistaler 2019), and the tropospheric stability framework (Ceppi and Gregory 2019). These three frameworks are bivariate frameworks. We show in this section that these three frameworks are actually particular cases of the multivariate decomposition described by Eq. (9). As a consequence, they all lead to an expression of the radiative response of Earth, which is the sum of two terms, 1) the response to the global mean surface temperature and 2) the response due to the pattern effect, as in the multivariate frameworks developed in the previous sections. However, since these alternative bivariate frameworks use a different metric  $\mathbf{p}$  for the pattern effect, they lead to a different interpretation of the variations in the global climate feedback parameter. We detail this below.

### a. Heat uptake efficacy framework

In the heat uptake efficacy framework, the changing pattern in SST is related to the ocean heat uptake (Jimenez de la Cuesta 2023) and its effect on global mean temperature is modeled by introducing an ocean heat uptake efficacy factor  $\epsilon$  in Eq. (6). The resulting equation for the global energy budget is the following [see, e.g., Eq. (9) in Held et al. (2010)]:

$$C \frac{d\tilde{T}}{dt} - \lambda_{ss} \tilde{T} = \tilde{F} - \epsilon \tilde{H}. \quad (20)$$

Note that when the efficacy factor equals 1, Eq. (20) represents the classical energy budget with a constant global climate feedback parameter [i.e., Eq. (6)]. Therefore, it is the distance of  $\epsilon \tilde{H}$  to  $\tilde{H}$  that represents the pattern effect rather than  $\epsilon \tilde{H}$ . In other words, the pattern effect is actually quantified by  $(\epsilon - 1) \tilde{H}$  rather than  $\epsilon \tilde{H}$  in Eq. (20). Equation (20) can

be rewritten to emphasize the role of the pattern effect in the following way:

$$C \frac{d\tilde{T}}{dt} - \lambda_{ss} \tilde{T} - (1 - \epsilon) \tilde{H} = \tilde{F} - \tilde{H}. \quad (21)$$

From Eq. (21), we see that the efficacy framework is a particular case of the multivariate energy budget represented by Eq. (10) where the ocean heat uptake  $H$  is used as the metric  $p$  for the pattern effect and where the radiative response change for a unit of change in ocean heat uptake is  $\partial_H R|_{(T,H)=(T_{ss},H_{ss})} = (1 - \epsilon)$ . The use of the change in ocean heat uptake as the metric for the pattern effect leads to a different interpretation of the variations in  $\lambda_v$  in the ocean heat uptake framework compared to our multivariate framework. Indeed, in the ocean heat uptake framework, the variations in  $\lambda_v$  are caused by variations in the ocean heat uptake in the following way:  $\lambda_v = [(1 - \epsilon) \tilde{H}] / T_{ss}$  while in the multivariate framework they are caused by variations in the SST [see Eq. (17)].

### b. Warm pool temperature framework

In the warm pool temperature framework, in addition to the average SST, the difference between the average and the warmest tropical waters (above which deep atmospheric convection occurs) plays a key role in the Earth albedo changes. Indeed, the temperature of the warmest 30% minus the tropical average SST (called  $\tilde{T}^\#$ ) exerts a control on the tropical average boundary layer capping strength by controlling the average temperature difference between the boundary layer and overlying free troposphere (through atmospheric convection; see Fueglistaler 2019). Since eastern Pacific low-level clouds are sensitive to boundary layer capping strength,  $\tilde{T}^\#$  changes affect tropical average albedo independently from average surface temperature changes. This adds on to the radiative response anomaly induced by global mean temperature changes in the following way:

$$\tilde{R} = \lambda_{ss} \tilde{T} + \gamma \tilde{T}^\#, \quad (22)$$

where  $\gamma$  is the sensitivity of the shortwave cloud radiative effect to  $\tilde{T}^\#$  ( $\gamma \sim -4.8 \text{ W m}^{-2} \text{ K}^{-1}$ , Fueglistaler 2019). The resulting equation for the global energy budget is the following:

$$C \frac{d\tilde{T}}{dt} - \lambda_{ss} \tilde{T} - \gamma \tilde{T}^\# = \tilde{F} - \tilde{H}. \quad (23)$$

From Eqs. (22) to (23), we see that the warm pool framework is a particular case of the multivariate energy budget represented by Eq. (10) where the relative temperature of the warmest tropical waters  $\tilde{T}^\#$  is used as the metric  $p$  for the pattern effect and where the radiative response change for a unit of change in  $\tilde{T}^\#$  is  $\partial_{T^\#} R|_{(T,T^\#)=(T_{ss},T_{ss}^\#)} = \gamma$ .

The use of the warmest tropical waters  $\tilde{T}^\#$  as the metric for the pattern effect leads to a different interpretation of the variations in  $\lambda_v$  in the warm pool framework compared to the multivariate framework here. Indeed, in the warm pool framework, the variations in  $\lambda_v$  are caused by variations in the

warmest tropical waters only:  $\tilde{\lambda}_v = \gamma \tilde{T}^\# / T_{ss}$ , while in the multivariate framework they are caused by variations in the SST over the whole ocean [see Eq. (17)].

### c. Tropospheric stability framework

In the tropospheric stability framework (Ceppi and Gregory 2019), the tropical boundary layer capping strength is represented by the estimated inversion strength (Wood and Bretherton 2006) rather than by  $\tilde{T}^\#$ . In this case, the equation for the global energy budget is the following [see Eq. (4) in Ceppi and Gregory (2019)]:

$$C \frac{d\tilde{T}}{dt} - \lambda_{ss} \tilde{T} - \sigma \tilde{S} = \tilde{F} - \tilde{H}, \quad (24)$$

where  $\tilde{S}$  is the area-averaged estimated inversion strength anomaly over oceanic regions equatorward of  $50^\circ$  and  $\sigma$  is the sensitivity of the shortwave cloud radiative effect to  $\tilde{S}$  ( $\sigma \sim -4 \text{ W m}^{-2} \text{ K}^{-1}$ ; Ceppi and Gregory 2019).

From Eq. (24), we see that the tropospheric stability framework is a particular case of the multivariate energy budget represented by Eq. (10) where  $\tilde{S}$  is used as the metric  $\mathbf{p}$  for the pattern effect and where the radiative response change for a unit of change in  $\tilde{S}$  is  $\partial_{\tilde{S}} R|_{(T,S)=(T_{ss},S_{ss})} = \sigma$ .

The use of the estimated inversion strength as the metric for the pattern effect leads to a different interpretation of the variations in  $\lambda_v$  in the tropospheric stability framework compared to our multivariate framework. Indeed, in the tropospheric stability framework, the variations in  $\lambda_v$  are caused by variations in the tropical boundary layer capping strength in the following way:  $\lambda_v = \sigma \tilde{S} / T_{ss}$ , while in the multivariate framework they are caused by variations in the SST directly [see Eq. (17)].

## 8. Discussion and conclusions

In this work we show that the classical approach to account for the pattern effect in EBMs, which simply consists in making the global climate feedback parameter  $\lambda$  be a variable that depends on the pattern of warming [see Eq. (8)] and which can be estimated as  $\lambda_v = \tilde{R} / \tilde{T}$  leads to two issues. First, it leads to large variations in  $\lambda_v$  of  $>+15\%$ , which violates assumptions that were made to develop the EBM in the first place. Second, the variations in  $\lambda_v$  get extreme and nonphysical when  $\tilde{T} \sim 0$ .

We revisit the development of the EBM from its original formulation, accounting for the dependence of the Earth radiative response anomaly  $\tilde{R}$  on both the global mean surface temperature and the pattern effect with a multivariate Taylor expansion of  $\tilde{R}$ . We show that the multivariate linearization of  $\tilde{R}$  is sufficient to accurately reproduce the Earth radiative response anomaly and the global mean surface temperature under abrupt  $4\text{CO}_2$  warming up to 5 K.

We evaluate the multivariate Earth radiative response anomaly in terms of variable global climate feedback parameter  $\lambda_v$ . We find the Earth radiative response anomaly is not the multiplication of  $\lambda_v$  by the global surface temperature anomaly  $\tilde{T}$  as in the classical framework but rather the sum of two terms: 1) the radiative response to the global mean

surface temperature and 2) the radiative response to the pattern of SST keeping the global mean temperature constant. This new expression of the Earth radiative response anomaly enables us to derive a new expression of  $\lambda_v : \lambda_v = \lambda_{ss} + (\tilde{R} - \lambda_{ss} \tilde{T}) / T_{ss}$ . This new expression of  $\lambda_v$  leads to variations in  $\lambda_v$  that are two orders of magnitude smaller than  $\lambda_{ss}$  for any value of  $\tilde{T}$ , meaning that assumptions made to derive the EBM are not violated and the EBM is self-consistent. This gives confidence in the physical grounding of the multivariate EBM.

With the multivariate framework, we also analyze the variations of the planetary heat uptake  $N = \tilde{F} + \tilde{R}$  as a function of the global mean surface temperature and the variable climate feedback parameter through a 3D generalization of the Gregory plot. We show that the apparent nonlinear behavior of  $\tilde{R}$  against  $\tilde{T}$  seen on the 2D Gregory plots of the classical energy budget can actually be explained by a bilinear dependence of  $\tilde{R}$  on the two variables  $\tilde{T}$  and the pattern of warming measured here by  $\tilde{\lambda}_v$ . The bilinear approximation is sufficient to represent accurately the Earth radiative response anomaly under abrupt  $4\text{CO}_2$  warming up to 5 K.

The 3D generalization of the Gregory plot shows that the expression  $\tilde{R} / \tilde{T}$  provides a measure of the global climate feedback parameter  $\lambda_v$  only when the pattern effect is close to 0. When the pattern effect is not close to 0 the expression  $\lambda_{ss} + (\tilde{R} - \lambda_{ss} \tilde{T}) / T_{ss}$  should be used instead to evaluate the global climate feedback parameter. This new expression of the global climate feedback parameter has profound consequences in particular on the definition of the climate sensitivity and its dependence on the pattern effect.

There is another interesting benefit of the multivariate EBM. It provides an explicit dependence of the global energy budget and the global climate feedback parameter on both the climate state  $\lambda_{ss}$  and the pattern effect. It enables us to disentangle the pattern effect from the climate state dependence. It also enables us to intercompare different simulations with different climate state references (through different  $\lambda_{ss}$ ), which holds promise to better quantify the relationship between the global energy budget of paleoclimates with the present-day global energy budget.

In section 4 we validated numerically the multivariate linearization of the Earth radiative response with only one AOGCM (CCSM4.0) and only over the first 150 years of an abrupt  $4\text{CO}_2$  simulation. Simulations from more models are needed to verify numerically the multivariate energy budget over other AOGCMs. To do this, piSST, piSST-pxK, and Green's function simulations from more AOGCMs models are needed. We also need LongRunMIP simulations (Rugenstein et al. 2019) from the same AOGCMs to test the multivariate linearization over longer time scales and warmer states in order to determine the limits of the multivariate linearization that are not yet seen over the first 150 years of abrupt  $4\text{CO}_2$  simulation.

**Acknowledgments.** We acknowledge the World Climate Research Programme's Working Group on Coupled Modelling, which is responsible for CMIP, and we thank the

climate modeling groups for producing and making available their model output, particularly those participating to the CFMIP project. We thank Maria Rugenstein and Jonah Bloch-Johnson for gathering LongRunMIP data and making them easily accessible. We thank Robin Chadwick for providing data from the CFMIP pilot experiments. We thank Yue Dong for making her Green's functions results available online. We also thank Jonathan Chenal for insightful comments and discussions.

**Data availability statement.** For IPSL-CM6A-LR, CESM2, and CNRM-CM6-1, we used abrupt-4xCO<sub>2</sub> simulation data from the Coupled Model Intercomparison Project (CMIP6) DECK experiments and the LongRunMIP experiments. Forcing data were computed using experiments from the Radiative Forcing Model Intercomparison Project (RFMIP) and  $\lambda_{ss}$  were computed with experiments from the Cloud Feedback Model Intercomparison Project (CFMIP). Additional data for HadGEM2-ES were provided by Robin Chadwick for the forcing and  $\lambda_{ss}$  while the abrupt-4xCO<sub>2</sub> are from the LongRunMIP simulations. All CMIP6 data are available on the Earth System Grid Foundation website <https://esgf.llnl.gov/>. LongRunMIP data information can be found at <http://www.LongRunMIP.org/>. CAM4 Green's functions data are available on Yue Dong's website <https://sites.google.com/view/yuedong-atmos/data>.

## APPENDIX

### The Global Energy Budget with a Variable $\lambda$ Derived with the Feedback Analysis Approach

A classical approach to derive the equations of the dynamics of the global energy budget is the feedback analysis. Here we follow the feedback analysis proposed by Roe (2009) in which we introduce a dependence of the feedbacks upon the geographical pattern of SST. We show that this approach leads to Eq. (10) for the dynamics of the global energy budget.

As in Roe (2009), we choose the idealization of a blackbody planet as a reference for the feedback analysis. In the absence of an atmosphere,  $S$ , the incoming shortwave radiation at the top of atmosphere (TOA) is a constant that depends on the albedo and the solar constant. The term  $I$ , the outgoing longwave radiation at TOA, is governed by the Stefan-Boltzman equation:

$$I = \sum_x \sigma T_x^4, \quad (A1)$$

where  $x$  indicates the geographical location. From Eq. (A1), we find that  $I = I(T, p)$  depends on both the global mean surface temperature  $T$  and the geographical pattern of temperature  $\mathbf{p}$ . In response to an anomalous radiative forcing  $\tilde{F}$ , the atmosphere and the surface radiation balance adjusts such that  $dR = \tilde{F}$ . Hence, in the reference blackbody system,  $\tilde{F}$  generates a change in global surface temperature  $dT$  and in SST pattern  $d\mathbf{p}$  such that:

$$\begin{aligned} dT &= \frac{\partial T}{\partial R} \Big|_{T=T_{ss}, \mathbf{p}=\mathbf{p}_{ss}} dR \Big|_{\mathbf{p}=\mathbf{p}_{ss}} = \frac{\partial T}{\partial I} \Big|_{T=T_{ss}, \mathbf{p}=\mathbf{p}_{ss}} dI \Big|_{\mathbf{p}=\mathbf{p}_{ss}} \\ &= \xi_0 dR \Big|_{\mathbf{p}=\mathbf{p}_{ss}}, \end{aligned} \quad (A2)$$

$$\begin{aligned} d\mathbf{p} &= \frac{\partial \mathbf{p}}{\partial R} \Big|_{T=T_{ss}, \mathbf{p}=\mathbf{p}_{ss}} dR \Big|_{T=T_{ss}} = \frac{\partial \mathbf{p}}{\partial I} \Big|_{T=T_{ss}, \mathbf{p}=\mathbf{p}_{ss}} dI \Big|_{T=T_{ss}} \\ &= \Gamma_0 dR \Big|_{T=T_{ss}}, \end{aligned} \quad (A3)$$

$$\begin{aligned} \tilde{F} &= dR = \frac{\partial I}{\partial T} \Big|_{T=T_{ss}, \mathbf{p}=\mathbf{p}_{ss}} dT + \frac{\partial I}{\partial \mathbf{p}} \Big|_{T=T_{ss}, \mathbf{p}=\mathbf{p}_{ss}} d\mathbf{p} \\ &= \frac{1}{\xi_0} dT + \frac{1}{\Gamma_0} d\mathbf{p}. \end{aligned} \quad (A4)$$

Note that the two constants  $\xi_0$  and  $\Gamma_0$  can be deduced from Eq. (A1) by decomposing  $T_x$  as combination of  $T$  and  $\mathbf{p}$ . In general terms, Eq. (A2) means that the blackbody reference system takes a perturbation in the forcing  $\tilde{F}$  and converts it into a response  $dT$  and  $d\mathbf{p}$ , which generates an output  $dR$  (see Fig. A1a). Now, let us consider a system closer to the real climate system in which there are feedbacks. A feedback is a process that makes the forcing a function of the response (that is, the process tends to amplify the original forcing because some fraction of the output is fed back into the input; see Fig. A1b). In the Earth climate, there are four important feedbacks: the water vapor feedback, the lapse rate feedback, the cloud feedback, and the surface albedo feedback. Each of these feedbacks is positive: they correspond to a response of the climate system to the increase in temperature, which tends to dampen the blackbody radiative response, leading to more warming such that the radiative perturbation can be compensated. When a feedback process is included in the system, the radiative perturbation to the system gets an additional nudge that is a function of the system response. At first order in  $dT$  and  $d\mathbf{p}$ , this nudge can be estimated as a linear function of the system response  $dT$  or  $d\mathbf{p}$  (see Figs. A1b,c). The system response now reads as follows:

$$dT = \xi_0 \left[ \tilde{F} + \sum_i (c_i dT + d_i d\mathbf{p}) - \frac{1}{\Gamma_0} d\mathbf{p} \right], \quad (A5)$$

$$d\mathbf{p} = \Gamma_0 \left[ \tilde{F} + \sum_i (c_i dT + d_i d\mathbf{p}) - \frac{1}{\xi_0} dT \right]. \quad (A6)$$

The system gets to a new steady state when the radiative response  $dR$  equals the radiative anomaly  $\tilde{F}$ . Solving for  $dR$  in Eq. (A5) or in Eq. (A6) leads to

$$dR = \tilde{F} = dT \left( \frac{1 - \sum_i f_i}{\xi_0} \right) + d\mathbf{p} \left( \frac{1 - \sum_i g_i}{\Gamma_0} \right), \quad (A7)$$

where  $f_i = \xi_0 c_i$  and  $g_i = \Gamma_0 d_i$  are constants that characterize the feedback of process  $i$ . Equation (A7) is strictly equivalent to Eq. (9) and thus leads to Eq. (10) for the dynamics of the global energy budget.

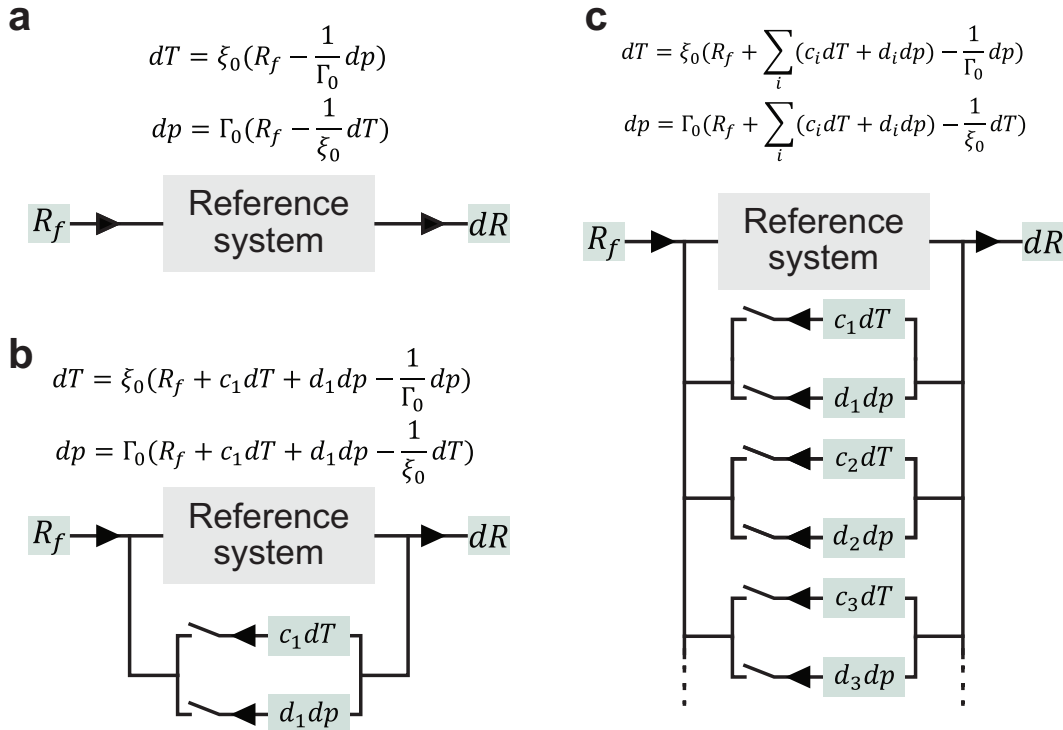


FIG. A1. Schematic illustration of the feedback analysis of the multivariate energy budget of the climate system: (a) reference system only, (b) one feedback, and (c) multiple feedbacks. The feedback loops take some fraction of the system output and feeds it back into the system input [adapted from Roe (2009)].

## REFERENCES

Andrews, T., and M. J. Webb, 2018: The dependence of global cloud and lapse rate feedbacks on the spatial structure of tropical Pacific warming. *J. Climate*, **31**, 641–654, <https://doi.org/10.1175/JCLI-D-17-0087.1>.

—, J. M. Gregory, and M. J. Webb, 2015: The dependence of radiative forcing and feedback on evolving patterns of surface temperature change in climate models. *J. Climate*, **28**, 1630–1648, <https://doi.org/10.1175/JCLI-D-14-00545.1>.

—, and Coauthors, 2018: Accounting for changing temperature patterns increases historical estimates of climate sensitivity. *Geophys. Res. Lett.*, **45**, 8490–8499, <https://doi.org/10.1029/2018GL078887>.

—, C. J. Smith, G. Myhre, P. M. Forster, R. Chadwick, and D. Ackerley, 2021: Effective radiative forcing in a GCM with fixed surface temperatures. *J. Geophys. Res. Atmos.*, **126**, e2020JD033880, <https://doi.org/10.1029/2020JD033880>.

Armour, K. C., 2017: Energy budget constraints on climate sensitivity in light of inconsistent climate feedbacks. *Nat. Climate Change*, **7**, 331–335, <https://doi.org/10.1038/nclimate3278>.

—, C. M. Bitz, and G. H. Roe, 2013: Time-varying climate sensitivity from regional feedbacks. *J. Climate*, **26**, 4518–4534, <https://doi.org/10.1175/JCLI-D-12-00544.1>.

Bloch-Johnson, J., M. Rugenstein, and D. S. Abbot, 2020: Spatial radiative feedbacks from internal variability using multiple regression. *J. Climate*, **33**, 4121–4140, <https://doi.org/10.1175/JCLI-D-19-0396.1>.

Budyko, M. I., 1969: The effect of solar radiation variations on the climate of the Earth. *Tellus*, **21**, 611–619, <https://doi.org/10.1111/j.2153-3490.1969.tb00466.x>.

Ceppi, P., and J. M. Gregory, 2019: A refined model for the Earth's global energy balance. *Climate Dyn.*, **53**, 4781–4797, <https://doi.org/10.1007/s00382-019-04825-x>.

Chadwick, R., H. Douville, and C. B. Skinner, 2017: Timeslice experiments for understanding regional climate projections: Applications to the tropical hydrological cycle and European winter circulation. *Climate Dyn.*, **49**, 3011–3029, <https://doi.org/10.1007/s00382-016-3488-6>.

Chenal, J., B. Meyssignac, A. Ribes, and R. Guillaume-Castel, 2022: Observational constraint on the climate sensitivity to atmospheric CO<sub>2</sub> concentrations changes derived from the 1971–2017 global energy budget. *J. Climate*, **35**, 4469–4483, <https://doi.org/10.1175/JCLI-D-21-0565.1>.

Dong, Y., C. Proistescu, K. C. Armour, and D. S. Battisti, 2019: Attributing historical and future evolution of radiative feedbacks to regional warming patterns using a Green's function approach: The preeminence of the western Pacific. *J. Climate*, **32**, 5471–5491, <https://doi.org/10.1175/JCLI-D-18-0843.1>.

Fueglistaler, S., 2019: Observational evidence for two modes of coupling between sea surface temperatures, tropospheric temperature profile, and shortwave cloud radiative effect in the tropics. *Geophys. Res. Lett.*, **46**, 9890–9898, <https://doi.org/10.1029/2019GL083990>.

Geoffroy, O., D. Saint-Martin, D. J. Olivié, A. Volodire, G. Bellon, and S. Tytéca, 2013a: Transient climate response in a two-layer energy-balance model. Part I: Analytical solution and parameter calibration using CMIP5 AOGCM experiments. *J. Climate*, **26**, 1841–1857, <https://doi.org/10.1175/JCLI-D-12-00195.1>.

—, —, G. Bellon, A. Volodire, D. J. L. Olivé, and S. Tytéca, 2013b: Transient climate response in a two-layer energy-balance model. Part II: Representation of the efficacy of deep-ocean heat uptake and validation for CMIP5 AOGCMs. *J. Climate*, **26**, 1859–1876, <https://doi.org/10.1175/JCLI-D-12-00196.1>.

Gregory, J. M., and P. Forster, 2008: Transient climate response estimated from radiative forcing and observed temperature change. *J. Geophys. Res.*, **113**, D23105, <https://doi.org/10.1029/2008JD010405>.

—, and T. Andrews, 2016: Variation in climate sensitivity and feedback parameters during the historical period. *Geophys. Res. Lett.*, **43**, 3911–3920, <https://doi.org/10.1002/2016GL068406>.

—, and Coauthors, 2004: A new method for diagnosing radiative forcing and climate sensitivity. *Geophys. Res. Lett.*, **31**, L03205, <https://doi.org/10.1029/2003GL018747>.

Hansen, J., and Coauthors, 2005: Efficacy of climate forcings. *J. Geophys. Res.*, **110**, D18104, <https://doi.org/10.1029/2005JD00576>.

Held, I. M., M. Winton, K. Takahashi, T. Delworth, F. Zeng, and G. K. Vallis, 2010: Probing the fast and slow components of global warming by returning abruptly to preindustrial forcing. *J. Climate*, **23**, 2418–2427, <https://doi.org/10.1175/2009JCLI346.1>.

Jimenez de la Cuesta, D., 2023: The varying Earth's radiative feedback connected to the ocean energy uptake: A theoretical perspective from conceptual frameworks. *J. Climate*, **36**, 2367–2385, <https://doi.org/10.1175/JCLI-D-22-0345.1>.

Lewis, N., and J. Curry, 2018: The impact of recent forcing and ocean heat uptake data on estimates of climate sensitivity. *J. Climate*, **31**, 6051–6071, <https://doi.org/10.1175/JCLI-D-17-0667.1>.

Loeb, N. G., T. J. Thorsen, J. R. Norris, H. Wang, and W. Su, 2018: Changes in Earth's energy budget during and after the “pause” in global warming: An observational perspective. *Climate*, **6**, 62, <https://doi.org/10.3390/cli6030062>.

Marvel, K., R. Pincus, G. A. Schmidt, and R. L. Miller, 2018: Internal variability and disequilibrium confound estimates of climate sensitivity from observations. *Geophys. Res. Lett.*, **45**, 1595–1601, <https://doi.org/10.1002/2017GL076468>.

Meyssignac, B., J. Chenal, N. G. Loeb, R. Guillaume-Castel, and A. Ribes, 2023: Time-variations of the climate feedback parameter  $\lambda$  are associated with the Pacific Decadal Oscillation. *Commun. Earth Environ.*, **4**, 241, <https://doi.org/10.1038/s43247-023-00887-2>.

Murphy, J. M., 1995: Transient response of the Hadley Centre coupled ocean–atmosphere model to increasing carbon dioxide. Part I: Control climate and flux adjustment. *J. Climate*, **8**, 36–56, [https://doi.org/10.1175/1520-0442\(1995\)008<0036:TROTH>2.0.CO;2](https://doi.org/10.1175/1520-0442(1995)008<0036:TROTH>2.0.CO;2).

—, and J. F. B. Mitchell, 1995: Transient response of the Hadley Centre coupled ocean–atmosphere model to increasing carbon dioxide. Part II: Spatial and temporal structure of response. *J. Climate*, **8**, 57–80, [https://doi.org/10.1175/1520-0442\(1995\)008<0057:TROTHC>2.0.CO;2](https://doi.org/10.1175/1520-0442(1995)008<0057:TROTHC>2.0.CO;2).

Neale, R. B., and Coauthors, 2010: Description of the NCAR Community Atmosphere Model (CAM5.0). NCAR Tech. Note NCAR/TN-486+STR, 268 pp., [www.cesm.ucar.edu/models/cesm1.1/cam/docs/description/cam5\\_desc.pdf](http://www.cesm.ucar.edu/models/cesm1.1/cam/docs/description/cam5_desc.pdf).

North, G. R., and K.-Y. Kim, 2017: *Energy Balance Climate Models*. Wiley, 392 pp.

Paynter, D., and T. L. Frölicher, 2015: Sensitivity of radiative forcing, ocean heat uptake, and climate feedback to changes in anthropogenic greenhouse gases and aerosols. *J. Geophys. Res. Atmos.*, **120**, 9837–9854, <https://doi.org/10.1002/2015JD023364>.

Roe, G., 2009: Feedbacks, timescales, and seeing red. *Annu. Rev. Earth Planet. Sci.*, **37**, 93–115, <https://doi.org/10.1146/annurev.earth.061008.134734>.

Rohrschneider, T., B. Stevens, and T. Mauritsen, 2019: On simple representations of the climate response to external radiative forcing. *Climate Dyn.*, **53**, 3131–3145, <https://doi.org/10.1007/s00382-019-04686-4>.

Rugenstein, M., and Coauthors, 2019: LongRunMIP: Motivation and design for a large collection of millennial-length AOGCM simulations. *Bull. Amer. Meteor. Soc.*, **100**, 2551–2570, <https://doi.org/10.1175/BAMS-D-19-0068.1>.

Sellers, W. D., 1969: A global climatic model based on the energy balance of the Earth–atmosphere system. *J. Appl. Meteor.*, **8**, 392–400, [https://doi.org/10.1175/1520-0450\(1969\)008<0392:AGCMBO>2.0.CO;2](https://doi.org/10.1175/1520-0450(1969)008<0392:AGCMBO>2.0.CO;2).

Senior, C. A., and J. F. B. Mitchell, 2000: The time-dependence of climate sensitivity. *Geophys. Res. Lett.*, **27**, 2685–2688, <https://doi.org/10.1029/2000GL011373>.

Sherwood, S. C., and Coauthors, 2020: An assessment of Earth's climate sensitivity using multiple lines of evidence. *Rev. Geophys.*, **58**, e2019RG000678, <https://doi.org/10.1029/2019RG000678>.

Storn, R., and K. Price, 1997: Differential evolution—a simple and efficient heuristic for global optimization over continuous spaces. *J. Global Optim.*, **11**, 341–359, <https://doi.org/10.1023/A:1008202821328>.

Taylor, K. E., R. J. Stouffer, and G. A. Meehl, 2012: An overview of CMIP5 and the experiment design. *Bull. Amer. Meteor. Soc.*, **93**, 485–498, <https://doi.org/10.1175/BAMS-D-11-00094.1>.

Webb, M. J., and Coauthors, 2017: The Cloud Feedback Model Intercomparison Project (CFMIP) contribution to CMIP6. *Geosci. Model Dev.*, **10**, 359–384, <https://doi.org/10.5194/gmd-10-359-2017>.

Winton, M., K. Takahashi, and I. M. Held, 2010: Importance of ocean heat uptake efficacy to transient climate change. *J. Climate*, **23**, 2333–2344, <https://doi.org/10.1175/2009JCLI3139.1>.

Wood, R., and C. S. Bretherton, 2006: On the relationship between stratiform low cloud cover and lower-tropospheric stability. *J. Climate*, **19**, 6425–6432, <https://doi.org/10.1175/JCLI3988.1>.

Zhang, B., M. Zhao, and Z. Tan, 2023: Using a Green's function approach to diagnose the pattern effect in GFDL AM4 and CM4. *J. Climate*, **36**, 1105–1124, <https://doi.org/10.1175/JCLI-D-22-0024.1>.

Zhou, C., M. D. Zelinka, and S. A. Klein, 2017: Analyzing the dependence of global cloud feedback on the spatial pattern of sea surface temperature change with a Green's function approach. *J. Adv. Model. Earth Syst.*, **9**, 2174–2189, <https://doi.org/10.1002/2017MS001096>.